# Decomposition of the Kennaugh Matrix Based on a New Norm

Biao You, Jian Yang, Junjun Yin, and Bin Xu

***Abstract*—In this letter, a new method for Kennaugh matrix decomposition is proposed, and a new norm for the Kennaugh matrix is defined. The Kennaugh matrix is decomposed into two parts: The first is a coherent target matrix, and the second is a residual matrix with minimum norm. The properties of the extracted coherent target are discussed, and an application of the extracted coherent target is implemented. In this application, an incoherent image is converted into a coherent image. Single-look sphere–diplane–helix decomposition is then performed. An experiment on Airborne SAR polarimetric data over San Francisco has been carried out, thus demonstrating the effectiveness of the application.**

***Index Terms*—Decomposition, Kennaugh matrix, polarimetry.**

## I. Introduction

EARLY radar systems were developed for detecting and ranging targets. With the development of synthetic aperture and polarimetric technology, modern polarimetric synthetic aperture radar (PolSAR) can capture the image and retrieve additional properties of the targets. The polarimetric scattering matrix, which is also known as the Sinclair matrix, contains essential target information in terms of electromagnetic field components [1], [2].

However, the scattered wave will be generally partially polarized, although the incident wave is monochromatic because the scattered wave is modulated by a "distributed target" [3]. A distributed target is described by multilook Kennaugh matrix $\mathbf{K}$, coherency matrix $\mathbf{T}$, or covariance matrix $\mathbf{C}$. If scattering matrix $\mathbf{S}$ is known, matrices $\mathbf{K}$, $\mathbf{T}$, or $\mathbf{C}$ can be easily obtained. However, the reverse is not necessarily true.

Huynen [4] decomposed a target into the sum of a coherent target (or a pure target, a single target, a point target) and an N-target. The coherent target corresponds to a scattering matrix, and the N-target is completely nonsymmetrical. Unfortunately, the Huynen decomposition is not stable, and the desired coherent target cannot be always obtained [5]. In [6], a coherent target was extracted from coherency matrix $\mathbf{T}$. However, the Frobenius norm was not appropriate for the aforementioned matrix.

Manuscript received May 28, 2013; revised August 5, 2013; accepted September 5, 2013. This work was supported in part by the National Natural Science Foundation of China under Grant 41171317 and in part by the Research Foundation of Tsinghua University.

The authors are with the Department of Electronic Engineering, School of Information Science and Technology, Tsinghua University, Beijing 100084, China (e-mail: youb09@mails.tsinghua.edu.cn; yangjian.ee@gmail.com; yinjj07@mails.tsinghua.edu.cn; xubin07161@gmail.com).

Color versions of one or more of the figures in this paper are available online at http://ieeexplore.ieee.org.

Digital Object Identifier 10.1109/LGRS.2013.2284336

In this letter, a new type of norm for the Kennaugh matrix is defined. Afterward, a new decomposition method is proposed. The Kennaugh matrix is decomposed into the sum of two matrices: The first is a Kennaugh matrix that corresponds to a coherent target, and the second is a residual matrix with minimum norm.

The properties of the extracted coherent target are discussed. The extracted target is the coherent target that is nearest to the original target. The extracted coherent target and the original target are almost the same in several polarimetric features (e.g., span).

A typical application of the extracted coherent target is implemented. The multilook polarimetric image is converted into a single-look image by using the proposed method. Multilook sphere–diplane–helix (SDH) decomposition [7] and single-look SDH decomposition methods [8] are then applied to both types of images. Comparisons are made between the two decomposition methods.

This letter is organized as follows. A number of preliminaries are presented in Section II. The new method for Kennaugh matrix decomposition is proposed in Section III. The properties of the extracted coherent target are discussed in Section IV. An application of the extracted coherent target is provided in Section V. The research is summarized in Section VI.

## II. Preliminaries

### A. Sinclair Matrix and Kennaugh Matrix

The coherent polarimetric target may be represented by a scattering matrix, i.e.,

$$\mathbf{S} = \begin{bmatrix} S_{HH} & S_{HV} \\ S_{VH} & S_{VV} \end{bmatrix} \tag{1}$$

where $S_{HV}$ denotes the complex scattering coefficient in the vertically transmitting and horizontally receiving channel, and the other three elements are defined similarly. Under the assumption of reciprocity, $S_{HV} = S_{VH}$; the Sinclair matrix can be transformed into a Pauli vector as follows:

$$\mathbf{k} = \frac{1}{\sqrt{2}} [\, S_{HH} + S_{VV} \quad S_{HH} - S_{VV} \quad 2S_{HV} \,]^T . \tag{2}$$

For the incoherent case, multilook coherency matrix $\mathbf{T}$ is often used, as in the following:

$$\mathbf{T} = \frac{1}{L} \sum_{i=1}^{L} \mathbf{k}_i \mathbf{k}_i^H \tag{3}$$

where $L$ is the number of looks, and superscript $H$ denotes the complex conjugate transpose. Matrix $\mathbf{T}$ is a $3 \times 3$ Hermitian matrix that is equivalent to a $4 \times 4$ real symmetrical Kennaugh matrix by (4) [9], as shown at the bottom of the page. For a coherent target, the Kennaugh matrix is related to the corresponding scattering matrix by

$$\mathbf{K} = \frac{1}{2}(\mathbf{Q})^{*}(\mathbf{S} \otimes \mathbf{S}^{*})\mathbf{Q}^{H} \tag{5}$$

with

$$\mathbf{Q} = \begin{bmatrix} 1 & 0 & 0 & 1 \\ 1 & 0 & 0 & -1 \\ 0 & 1 & 1 & 0 \\ 0 & -j & j & 0 \end{bmatrix}. \tag{6}$$

The symbol $\otimes$ denotes the Kronecker product, and superscript $*$ indicates the complex conjugate.

### *B. Huynen Decomposition and Lueneburg Approximation*

In his pioneering work on radar polarimetry [4], Huynen decomposed Kennaugh matrix $\mathbf{K}$ into two parts: The first part corresponds to a pure single target that is denoted by $\mathbf{K_0}$, and the second part corresponds to N-target $\mathbf{K_N}$, as shown in the following:

$$\mathbf{K} = \mathbf{K_0} + \mathbf{K_N}. \tag{7}$$

Coherent target $\mathbf{K_0}$ has five independent variables and can be transformed into a scattering matrix by using (5).

Lueneburg *et al.* [6] obtained scattering matrix $\mathbf{S}$ by minimizing

$$\|\mathbf{T} - c \cdot \mathbf{k} \cdot \mathbf{k}^{H}\|_{F} \tag{8}$$

where $\mathbf{T}$ is the coherency matrix of a distributed target, $c$ is a complex number, $\mathbf{k}$ is the Pauli vector of scattering matrix $\mathbf{S}$, and $\|\cdot\|_{F}$ stands for the Frobenius norm. Equation (8) is proven to be minimum only when $\mathbf{k}$ is equal to the eigenvector corresponding to the largest eigenvalue of matrix $\mathbf{T}$.

## III. Kennaugh Matrix Decomposition

### *A. Polarization Synthesis*

If the Kennaugh matrix is known, then the received power is the function of the transmitting and receiving antenna polarization states described as follows [10]:

$$\begin{aligned} &P(\chi_r, \psi_r, \chi_t, \psi_t) = \frac{4\pi}{k^2}\mathbf{J_r}^{T}\mathbf{K}\mathbf{J_t}, \\ &\mathbf{J_r} = [\,1 \quad \cos 2\chi_r \cos 2\psi_r \quad \cos 2\chi_r \sin 2\psi_r \quad \sin 2\chi_r\,]^{T}; \\ &\mathbf{J_t} = [\,1 \quad \cos 2\chi_t \cos 2\psi_t \quad \cos 2\chi_t \sin 2\psi_t \quad \sin 2\chi_t\,]^{T} \end{aligned} \tag{9}$$

where $\mathbf{J}$ is the Stokes vector, $\chi$ is the ellipticity angle ranging from $-(\pi/4)$ to $(\pi/4)$, $\psi$ is the orient angle ranging from $-(\pi/2)$ to $(\pi/2)$, subscripts $t$ and $r$ denote the transmitting and receiving antenna polarization states, respectively. Equation (9) can be rewritten into

$$\begin{aligned} &P(\chi_r, \psi_r, \chi_t, \psi_t) \\ &\quad = K_{11} + \cos 2\chi_t \cos 2\psi_t \cdot K_{12} \\ &\qquad + \cos 2\chi_t \sin 2\psi_t \cdot K_{13} + \sin 2\chi_t \cdot K_{14} \\ &\qquad + \cos 2\chi_r \cos 2\psi_r \cdot K_{21} + \cos 2\chi_t \cos 2\psi_t \cos 2\chi_r \cos 2\psi_r \\ &\qquad \cdot K_{22} + \cos 2\chi_t \sin 2\psi_t \cos 2\chi_r \cos 2\psi_r \cdot K_{23} \\ &\qquad + \sin 2\chi_t \cos 2\chi_r \cos 2\psi_r \cdot K_{24} + \cos 2\chi_r \sin 2\psi_r \\ &\qquad \cdot K_{31} + \cos 2\chi_t \cos 2\psi_t \cos 2\chi_r \sin 2\psi_r \cdot K_{32} \\ &\qquad + \cos 2\chi_t \sin 2\psi_t \cos 2\chi_r \sin 2\psi_r \cdot K_{33} \\ &\qquad + \sin 2\chi_t \cos 2\chi_r \sin 2\psi_r \cdot K_{34} + \sin 2\chi_r \cdot K_{41} \\ &\qquad + \cos 2\chi_t \cos 2\psi_t \sin 2\chi_r \cdot K_{42} + \cos 2\chi_t \sin 2\psi_t \sin 2\chi_r \\ &\qquad \cdot K_{43} + \sin 2\chi_t \sin 2\chi_r \cdot K_{44}. \end{aligned} \tag{10}$$

### *B. Norm of the Kennaugh Matrix*

From (10), we can see that each element of the Kennaugh matrix has different weight contributions to the receiving power. For example, element $K_{11}$ has the coefficient 1, and element $K_{12}$ has the coefficient $\cos 2\chi_t \cos 2\psi_t$, etc. Thus, we define the square of the Kennaugh matrix norm as

$$\begin{aligned} \|\mathbf{K}\|_{K}^{2} &\triangleq \langle 1^2 \cdot K_{11}^2 + (\cos 2\chi_t \cos 2\psi_t)^2 K_{12}^2 \\ &\qquad + \cdots + (\sin 2\chi_t \sin 2\chi_r)^2 K_{44}^2 \rangle \\ &= K_{11}^2 + \frac{1}{4}K_{12}^2 + \frac{1}{4} \cdot K_{13}^2 + \frac{1}{2}K_{14}^2 \\ &\quad + \frac{1}{4}K_{21}^2 + \frac{1}{16}K_{22}^2 + \frac{1}{16}K_{23}^2 + \frac{1}{8}K_{24}^2 \\ &\quad + \frac{1}{4}K_{31}^2 + \frac{1}{16}K_{32}^2 + \frac{1}{16}K_{33}^2 + \frac{1}{8}K_{34}^2 \\ &\quad + \frac{1}{2}K_{41}^2 + \frac{1}{8}K_{42}^2 + \frac{1}{8}K_{43}^2 + \frac{1}{4}K_{44}^2 \\ &= \sum_{1 \le i,j \le 4} a_{ij} K_{ij}^2 \end{aligned} \tag{11}$$

where $\langle \cdot \rangle$ indicates an average over all possible polarimetric states $(\chi_r,\ \psi_r)$ and $(\chi_t,\ \psi_t)$, and subscript $K$ indicates that the norm is defined for the Kennaugh matrix.

### *C. Norm of the Coherency Matrix*

From (4), a one-to-one correspondence $f(\cdot)$ is observed between coherency matrix $\mathbf{T}$ and Kennaugh matrix $\mathbf{K}$, such that

$$f(\mathbf{T}) = \mathbf{K} \tag{12}$$

$$f^{-1}(\mathbf{K}) = \mathbf{T}. \tag{13}$$

$$\mathbf{K} = \begin{bmatrix} \frac{T_{11}+T_{22}+T_{33}}{2} & \mathrm{Re}(T_{12}) & \mathrm{Re}(T_{13}) & \mathrm{Im}(T_{23}) \\ \mathrm{Re}(T_{12}) & \frac{T_{11}+T_{22}-T_{33}}{2} & \mathrm{Re}(T_{23}) & \mathrm{Im}(T_{13}) \\ \mathrm{Re}(T_{13}) & \mathrm{Re}(T_{23}) & \frac{T_{11}-T_{22}+T_{33}}{2} & -\mathrm{Im}(T_{12}) \\ \mathrm{Im}(T_{23}) & \mathrm{Im}(T_{13}) & -\mathrm{Im}(T_{12}) & \frac{-T_{11}+T_{22}+T_{33}}{2} \end{bmatrix} \tag{4}$$

Given coherency matrix $\mathbf{T}$, we define its norm as

$$\|\mathbf{T}\|_T \triangleq \|f(\mathbf{T})\|_K \tag{14}$$

where subscript $T$ indicates that the norm is defined for the coherency matrix. Substituting (4) into (11), the square of the coherency matrix $\mathbf{T}$ norm should be defined as

$$\begin{aligned}\|\mathbf{T}\|_T^2 = &\frac{11}{32}T_{11}^2 + \frac{11}{32}T_{22}^2 + \frac{11}{32}T_{33}^2 + \frac{3}{8}T_{11}T_{22} \\ &+ \frac{3}{8}T_{11}T_{33} + \frac{9}{16}T_{22}T_{33} + \frac{1}{2}\left(\mathrm{Re}(T_{12})\right)^2 \\ &+ \frac{1}{2}\left(\mathrm{Re}(T_{13})\right)^2 + \frac{1}{8}\left(\mathrm{Re}(T_{23})\right)^2 + \frac{1}{4}\left(Im(T_{12})\right)^2 \\ &+ \frac{1}{4}\left(Im(T_{13})\right)^2 + \left(Im(T_{23})\right)^2. \end{aligned} \tag{15}$$

From this point of view, the norm $\|\mathbf{T}\|_T$ that is derived from $\|\mathbf{T}\|_K$ is more appropriate than the Frobenius norm. Function $\|\cdot\|_T$, which is defined in (15), satisfies the three conditions of a norm (see the Appendix for proof).

### D. New Decomposition of the Kennaugh Matrix

Similar to Huynen's work, we decompose the Kennaugh matrix into two parts, i.e.,

$$\mathbf{K} = \mathbf{K^0} + \Delta\mathbf{K}. \tag{16}$$

Matrix $\mathbf{K^0}$ is a pure single target corresponding to scattering matrix $\mathbf{S}$, and matrix $\Delta\mathbf{K}$ is a noise matrix. Then, we try to find matrix $\mathbf{S}$, such that the following norm is minimum:

$$\begin{aligned}\|\Delta\mathbf{K}\|_K &= \|\mathbf{K} - \mathbf{K^0}\|_K \\ &= \left\|\mathbf{K} - \frac{1}{2}(\mathbf{Q})^*(\mathbf{S}\otimes\mathbf{S}^*)\mathbf{Q}^{\mathbf{H}}\right\|_K. \end{aligned} \tag{17}$$

The aforementioned three methods can be used to derive a coherent target from the incoherent target. The pure single target $\mathbf{K}_0$ that is derived from the Huynen decomposition has a clear meaning. The elements in $\mathbf{K}_0$ are called "Huynen parameters." Each element has an important role in target information interpretation. The eigenvector $\mathbf{k}$ that is derived from the Lueneburg approximation corresponds to the main scattering mechanism of the target. A detailed physical description of the proposed decomposition method will be discussed in the following section.

## IV. Properties of the Extracted Coherent Target

The extracted coherent target $\mathbf{K}^0$ that is derived from the proposed method is the pure single target that is "nearest to" the original incoherent target $\mathbf{K}$ (for an intuitive explanation, see Fig. 1). In this section, we will focus on the two properties of the extracted coherent target.

*Property 1:* The span of $\mathbf{K}^0$ is almost the same as the span of $\mathbf{K}$.

*Property 2:* Coherent target $\mathbf{K}^0$ often exhibits the same scattering mechanism as the original target $\mathbf{K}$. If the original target $\mathbf{K}$ exhibits surface (odd bounce) scattering, then target $\mathbf{K}^0$ also generally exhibits a surface scattering mechanism. The same is also true for double-bounce (even bounce) scattering.

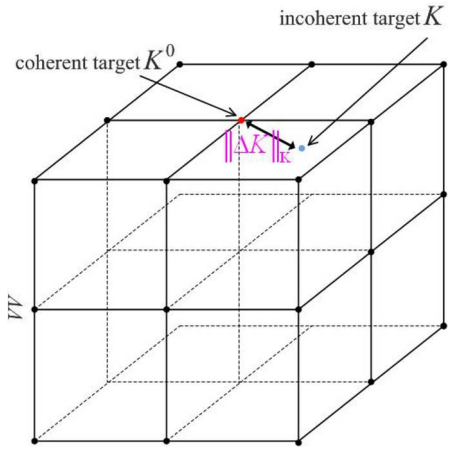


Fig. 1. Nearest coherent target to the incoherent target.

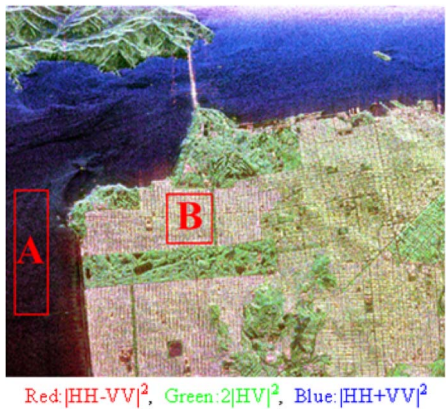


Fig. 2. Pauli decomposition of the experiment data.

We have chosen JPL Airborne SAR L-band PolSAR data over San Francisco as the experimental data set. The image size is 900 × 1024. The Pauli decomposition of this image is shown in Fig. 2. Two typical areas are selected. The left area A is a partition of the sea dominated by surface scattering. The right area B is in the urban section dominated by double-bounce scattering.

### A. Power Perseverance

The ratio of the power of the extracted coherent target to the original power of the pixel is compared. We define a new variable as follows:

$$R = \frac{\text{power of extracted coherence target}}{\text{original target power}}. \tag{18}$$

The entropy in Area A is extremely low, thus indicating that only one dominant scattering mechanism exists. The three methods have obtained extremely significant extracted power ratios in this area. In Area B, however, the entropy is remarkably higher. Most pixels contain more than one mechanism. In Table I, we can see that the proposed method has a significantly higher power ratio than the other two methods.

TABLE I
COMPARISON OF POWER RATIOS FOR DIFFERENT METHODS (IN PERCENTAGE)

| Method | Area A | Area B |
|---|---|---|
| Huynen's decomposition | 95.17 | 60.18 |
| Lueneburg's approximation | 95.69 | 78.89 |
| The proposed method | 97.88 | 91.21 |

TABLE II
COMPARISON OF THE RATIO OF THE POLARIMETRIC SCATTERING MECHANISM THAT REMAIN UNCHANGED FOR DIFFERENT METHODS (IN PERCENTAGE)

| Method | Area A | Area B |
|---|---|---|
| Huynen's decomposition | 100 | 33.98 |
| Lueneburg's approximation | 100 | 93.73 |
| The proposed method | 100 | 97.41 |

### *B. Polarimetric Scattering Characteristic Analysis*

In this section, we consider the properties of the polarimetric scattering characteristic of $\mathbf{K}^0$. $H/\alpha$ decomposition is applied to determine the scattering mechanism of each pixel [11], [12]. For an incoherent target, the $\alpha$ angle can be calculated as described in [11]. For coherent target $\mathbf{K}^0$, we first rewrite it in the form of a Pauli vector, as in the following:

$$\mathbf{k} = [k_1 \quad k_2 \quad k_3]^T. \tag{19}$$

The $\alpha$ angle of the coherent target is computed as

$$\alpha = \tan^{-1}\left(\frac{\sqrt{|k_2|^2 + |k_3|^2}}{|k_1|}\right). \tag{20}$$

A pixel is classified as the surface scattering if its $\alpha$ angle is smaller than 42.5°. A pixel is classified as the double-bounce scattering if its $\alpha$ angle is greater than 47.5° [3], [11].

In Area A, most of the original targets exhibit the surface scattering mechanism. We have calculated the extracted coherent target that also exhibits the surface scattering mechanism. The second column in Table II shows that the surface scattering mechanism of all surface scattering pixels in Area A remains unchanged after the three decomposition methods.

In Area B, most of the original targets exhibit the double-bounce scattering mechanism. We have calculated the extracted coherent target that also exhibits the double-bounce scattering mechanism. The last column in Table II shows that, for the incoherent double-bounce targets in Area B, only 33.98% of the extracted pure coherent targets retain double-bounce scattering using Huynen decomposition. The proposed method exhibits the highest ratio of unchanged double-bounce scattering characteristic in Area B. More than 97% of the pixels retain their scattering mechanism, and only a few pixels shift to a different scattering mechanism.

## V. APPLICATION OF THE EXTRACTED COHERENT TARGET

### *A. New Flowchart of Target Decomposition*

The new flowchart of target decomposition is presented in Fig. 3. Incoherent target decomposition (ICTD) is used for incoherent images that are described by a coherency or covariance matrix. Coherent target decomposition (CTD) is used for coherent images that are described by a scattering matrix.

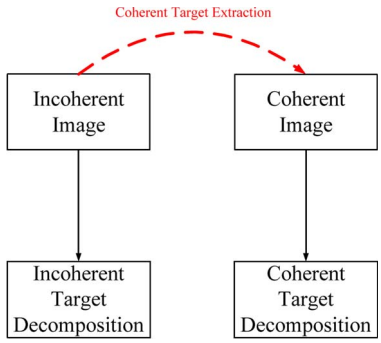


Fig. 3. New flowchart of target decomposition.

Using the proposed method, the coherent target that is nearest to the incoherent target has been obtained. Simultaneously, the incoherent PolSAR image has been converted into a coherent PolSAR image, and then, the CTD can be applied. With the help of coherent target extraction, the ICTD and the CTD have been connected.

In this section, two decomposition methods will be compared. The first method is the SDH decomposition for multilook polarimetric data [7]. In the second method, we initially extract the coherent target from the incoherent image, and then, the SDH decomposition for a single-look image is applied to the extracted image.

### *B. SDH Decomposition*

Krogager and Czy [8] decomposed scattering matrix $\mathbf{S}$ into the sum of three components as follows:

$$\mathbf{S} = e^{j\varphi}\left\{e^{j\varphi_s}k_s\mathbf{S}_{\text{sphere}} + k_d\mathbf{S}_{\text{diplane}(\theta)} + k_h\mathbf{S}_{\text{helix}(\theta)}\right\} \tag{21}$$

where $k_s$, $k_d$, and $k_h$ are the magnitudes of the sphere, the diplane, and the helix, respectively, as defined in the following:

$$\begin{aligned} k_s &= |S_{RL}| \\ k_d &= \min\left(|S_{RR}|, |S_{LL}|\right) \\ k_h &= \max\left(|S_{RR}|, |S_{LL}|\right) - \min\left(|S_{RR}|, |S_{LL}|\right) \end{aligned} \tag{22}$$

where $|S_{RR}|$, $|S_{RL}|$, and $|S_{LL}|$ are the elements in the right–left (R, L) circular basis, with

$$\begin{aligned} S_{RR} &= jS_{HV} + \frac{1}{2}(S_{HH} - S_{VV}) \\ S_{LL} &= jS_{HV} - \frac{1}{2}(S_{HH} - S_{VV}) \\ S_{RL} &= \frac{j}{2}(S_{HH} + S_{VV}). \end{aligned} \tag{23}$$

The SDH decomposition can be also extended for a multilook case [7], as in the following:

$$\begin{aligned} |S_{RL}| &= \sqrt{T_{11}} \\ |S_{RR}| &= \sqrt{T_{33} + jT_{32} - jT_{23} + T_{22}} \\ |S_{LL}| &= \sqrt{T_{33} - jT_{32} + jT_{23} + T_{22}}. \end{aligned} \tag{24}$$

Substituting (24) into (22) will complete the SDH decomposition for multilook data.

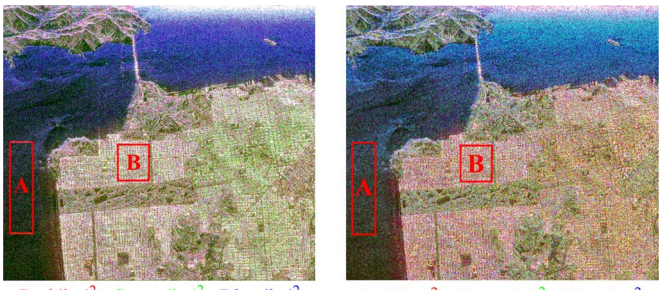


Fig. 4. (a) Multilook SDH decomposition of the experiment data. (b) Single-look SDH decomposition of the extracted coherent data.

TABLE III
THREE MECHANISM PROPORTIONS IN TWO AREAS USING THE TWO DECOMPOSITION METHODS (IN PERCENTAGE)

| Method | $P_s$ | $P_d$ | $P_h$ |
|---|---|---|---|
| Method 1, Area A | 86.5 | 12.0 | 1.4 |
| Method 1, Area B | 41.0 | 42.7 | 16.3 |
| Method 2, Area A | 89.4 | 7.0 | 3.4 |
| Method 2, Area B | 36.8 | 54.8 | 8.4 |

### C. Comparison Analysis

The results of the multilook SDH decomposition of the experiment data are presented in Fig. 4(a). The results of the single-look SDH decomposition of the extracted coherent data are presented in Fig. 4(b). The figures are color-coded as red for $|k_d|^2$, green for $|k_h|^2$, and blue for $|k_s|^2$. For each pixel, the three mechanism proportions are calculated as follows:

$$P_i = \frac{|k_i|^2}{|k_s|^2 + |k_d|^2 + |k_h|^2}, \quad i = s, d, h. \tag{25}$$

$P_s$, $P_d$, and $P_h$ stand for the mechanism proportions of the sphere, the diplane, and the helix, respectively.

For the pixels in Area A, the radar signal was reflected by the sea surface and was returned to the radar directly. The surface proportion $P_s$ in this area is expected to be significantly high. In this image, the illumination is from the top, and the flight motion is from left to right [13]. Area B is a residential area wherein most of the streets are parallel with the flight direction. The building and the streets can easily form a dihedral. Most pixels in Area B are characterized by a strong dihedral scattering component [14]. The dihedral proportion $P_d$ in this area is expected to be relatively high. The mean values of variables $P_s$, $P_d$, and $P_h$ in Areas A and B are listed in Table III. Note that the mean of $P_s$ in Area A and that of $P_d$ in Area B are 89.4% and 54.8%, respectively, in the last two lines of the table. Both numbers are larger than the corresponding numbers that are achieved by the first method, thus suggesting that the second decomposition method is remarkably reasonable. Compared with the incoherent method, the coherent method can provide more detailed polarimetric features.

## VI. SUMMARY

In this letter, we have defined a new norm for the Kennaugh matrix and have extracted a coherent target from an incoherent target. The extracted target is the nearest coherent target to the incoherent target. This extracted target has almost the same polarimetric characteristics as the original target. In essence, SAR is a coherent remote sensing technique. The scattering matrix is the fundamental element. The coherency matrix retains the second-order statistics of polarimetric information [15]. Multilook average will lose certain polarimetric features [16]. By extracting the nearest coherent target, the ICTD and the CTD are connected.

## APPENDIX

The function $\|\cdot\|_T$ that is defined in (15) satisfies the following three conditions:

1) $\|\mathbf{T}\|_T \geq 0$ and $\|\mathbf{T}\|_T = 0$ if and only if $\mathbf{T} = \mathbf{0}$.
2) $\alpha\|\mathbf{T}\|_T = |\alpha|\|\mathbf{T}\|_T$.
3) $\|\mathbf{T_x} + \mathbf{T_y}\|_T \leq \|\mathbf{T_x}\|_T + \|\mathbf{T_y}\|_T$.

The function $f(\cdot)$ in (12) can be easily verified as linearly transformed, as in the following:

$$\begin{aligned}\|\mathbf{T_x} + \mathbf{T_y}\|_T &= \|f(\mathbf{T_x} + \mathbf{T_y})\|_K = \|f(\mathbf{T_x}) + f(\mathbf{T_y})\|_K \\ &\leq \|f(\mathbf{T_x})\|_K + \|f(\mathbf{T_y})\|_K = \|\mathbf{T_x}\|_T + \|\mathbf{T_y}\|_T.\end{aligned}$$

Thus, condition (3) is proven. The other two conditions may be proven by using similar methods.

## REFERENCES

[1] J. R. Huynen, "The Stokes matrix parameters and their interpretation in terms of physical target properties," in *Proc. Journes Int. Polarimtrie Radar*, Nantes, France, Mar. 1990, pp. 195–207.
[2] E. Pottier, "On Dr J.R. Huynen's main contributions in the development of polarimetric radar techniques, and how the "radar targets phenomenological concept" becomes a theory," in *Proc. SPIE Radar Polarimetry*, 1992, vol. 1748, pp. 72–85.
[3] J. S. Lee and E. Pottier, *Polarimetric Radar Imaging: From Basics to Applications*. Boca Raton, FL, USA: CRC Press, 2009.
[4] J. R. Huynen, "Phenomenological theory of radar targets," Ph.D. dissertation, Tech. Univ. Delft, Delft, The Netherlands, 1970.
[5] J. Yang, "On theoretical problems in radar polarimetry," Ph.D. dissertation, Niigata Univ., Niigata, Japan, 1999.
[6] E. Lueneburg, M. Chandra, and W. M. Boerner, "Random target approximations," in *Proc. PIERS*, Noordwijk, The Netherlands, 1994, pp. 1366–1369.
[7] H. Wang, Q. Huang, and Y. Pi, "Polarization decomposition with S and T matrix of a PolSAR image," in *Proc. IEEE ICCCAS*, 2009, pp. 530–532.
[8] E. Krogager and Z. H. Czy, "Properties of the sphere, diplane, and helix decomposition," in *Proc. 3rd Int. Workshop Radar Polarimetry*, Nantes, France, Apr. 1995, pp. 106–114.
[9] S. R. Cloude, *Polarisation: Applications in Remote Sensing*. New York, NY, USA: Oxford Univ. Press, 2010.
[10] J. J. van Zyl, H. A. Zebker, and C. Elachi, "Imaging radar polarization signatures: Theory and observation," *Radio Sci.*, vol. 22, no. 4, pp. 529–543, Jul./Aug. 1987.
[11] S. R. Cloude and E. Pottier, "An entropy based classification scheme for land applications of polarimetric SAR," *IEEE Trans. Geosci. Remote Sens.*, vol. 35, no. 1, pp. 68–78, Jan. 1997.
[12] S. R. Cloude, "Radar target decomposition theorems," *Electron. Lett.*, vol. 21, no. 1, pp. 22–24, Jan. 1985.
[13] J. J. van Zyl, "Unsupervised classification of scattering behavior using radar polarimetry data," *IEEE Trans. Geosci. Remote Sens.*, vol. 27, no. 1, pp. 36–45, Jan. 1989.
[14] R. Zandoná Schneider, K. P. Papathanassiou, I. Hajnsek, and A. Moreira, "Polarimetric and interferometric characterization of coherent scatterers in urban areas," *IEEE Trans. Geosci. Remote Sens.*, vol. 44, no. 4, pp. 971–984, Apr. 2006.
[15] Y. Yamaguchi, A. Sato, W.-M. Boerner, R. Sato, and H. Yamada, "Four-component scattering power decomposition with rotation of coherency matrix," *IEEE Trans. Geosci. Remote Sens.*, vol. 49, no. 6, pp. 2251–2258, Jun. 2011.
[16] V. Alberga, G. Satalino, and D. K. Staykova, "Comparison of polarimetric SAR observables in terms of classification performance," *Int. J. Remote Sens.*, vol. 29, no. 14, pp. 4129–4150, Jul. 2008.